Check for updates

Electrically variable liquid crystal lenses for ophthalmic distance accommodation

T. GALSTIAN,[1,2,*] K. ASATRYAN,[2] V. PRESNIAKOV,[2] AND A. ZOHRABYAN[2]

[1]*Center for Optics, Photonics and Laser, Department of Physics, Engineering Physics and Optics, Université Laval, 2375 Rue de la Terrasse, Québec G1V 0A6, Canada*
[2]*TLCL Optical Research Inc. and Lensvector Inc., Canada*
*galstian@phy.ulaval.ca

Abstract: We present the example of a specific design of an electrically tunable liquid crystal lens (TLCL) with floating electrode to analyze experimentally the potential of using TLCLs in intraocular implants. An optimized voltage-frequency driving technique is demonstrated to achieve high optical powers (up to 4 diopters) with very low aberrations (below 0.1μm) for an optical aperture of 3mm. In addition, the continuous character of distance accommodation and the absence of granularity across the aperture of the lens (pixel-free) make this component an excellent choice for various ophthalmic applications.

1. Introduction

Age-related loss of human capacity of distance accommodation (presbyopia) is a well-known problem in ophthalmology (see, e.g., [1]). Various approaches have been proposed to address this issue, including the use of fixed multifocal intraocular lenses (IOLs) and accommodative IOLs (AIOLs) [2]. While there has been a significant progress in the design of the IOL's properties [3], the relative gain (thanks to the use of an AIOL versus, e.g., a monofocal IOL) remains to be proven [4]. Another open question is the evolution of the balance of mechanical forces (weakening of the ciliary muscle, rigidity changes of the lens and its environment) [5] needed to perform the accommodation function with most of the "muscularly activated" AIOLs available nowadays [2].

Alternative approaches have been suggested to fabricate electrically controlled AIOL assemblies without relying on mechanical movement or deformation [6–10]. Those solutions use the electric field induced refractive index changes [11] in nematic liquid crystals (NLCs) [12] to fabricate electrically tunable liquid crystal lenses (TLCLs). In the case where such TLCLs have relatively small diameters (see hereafter), they can be combined with a larger aperture (e.g., 6 mm) fixed focus monofocal IOL (see Fig. 1 and [10,13]) to provide dynamic phase changes only in the central portion of the optical system.
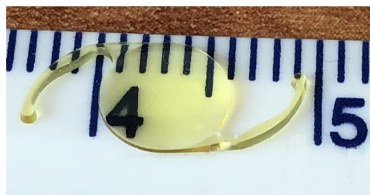
Fig. 1. Photography of a typical monofocal intraocular lens used in cataract surgery (minimum division is 1mm).

In fact, there have been at least three different families of TLCLs reported: 1- diffractive lenses (see, e.g., [8]), 2- refractive lenses using transversally non uniform thickness of the NLC, such as a plano convex or meniscus lens (see, e.g., [14]), and 3- gradient index "modal-control" lenses (see, e.g., [15,16]) that we would like to analyse in the present work in view of their potential use in an AIOL implant. Each of those approaches (to build TLCLs) has

advantages and drawbacks. Some of them (the refractive lens) have been already introduced into miniature cameras (in webcams and mobile phones [17,18]) and were analyzed from corresponding optical power (OP) and root mean square (RMS) aberrations point of views [16].

However, the above-mentioned characterization (focused mainly on the mobile camera requirements) is not enough to conclude about their relevance for ophthalmic application since the AIOL sets very specific requirements, including on the point spread function (PSF) as well as on scattering and halo effects, which are usually not characterized in most of previous publications. Indeed, the characterization of those TLCLs is often made within relatively narrow scopes and there are many questions remaining unanswered due to the lack of well-defined inquiries from the ophthalmic community. Consequently, scientific publications with such specific analysis for the correspondence of TLCLs to requirements of AIOL are still missing.

The current work aims 1- presenting to the scientific community the key criteria for the design of TLCL for ophthalmic (IOL) application, 2- investigating the TLCL approach that we have recently developed (using a floating electrode) and 3- answering several key questions (see Table 1) that might help ophthalmology experts to take decisions when considering various AIOL solutions.

We shall start by describing the geometry of the TLCL we have developed. We shall then provide its standard and optimized characterization data (OP's variability range and RMS aberrations). We shall also provide PSF measurement results, as well as optical performance (visual perception) data, including visual chart, light transmission and scattering that may affect the starburst and halo effects.

During the recent years, we have conducted intensive discussions and consultations with experts from ophthalmology community. This effort brought us to the following list of requirements (see Table 1) that must be satisfied for an electrically variable lens to qualify as a candidate for an AIOL application.

Table 1. Target specifications of the TLCL for AIOL application.

Parameter	Specification	Comment
Dynamic optical aperture (mm)	≥ 3	Must be combined with a fixed-focus IOL
Dynamic focusing range (Diopters)	≥ 4	This should cover almost 100% of patients
Default/Unpowered mode (Diopters)	0	Far distance vision at 0V (safety considerations)
Focusing accuracy (Diopters)	≤ 0.25	Distance resolution
RMS wavefront error (μm) High order aberrations	≤ 0.2 ≤ 0.1	Usual reference is $\lambda/4$
PSF (85% encircled energy radius [arcmin])	≤ 2	Acceptable acuity
Scattering (%)	≤ 5.5	Averaged between 450 nm – 650 nm
Transmission (%)	≥ 90	Averaged between 450 nm – 650 nm
Response time (sec)	≤ 1	1 cycle (far-near-far)
Electric power consumption (μW)	≤ 10	Only the lens
Thickness (mm)	≤ 1	Not critical
Starburst and halo level	$\leq$ Multifocal	Ideally must be comparable to monofocal IOLs

Most of the requirements (see parameters listed in Table 1) are rather simple to justify since they are directly related to the eye optics, while some others would need additional explanations. Namely, the human iris can expand up to 6mm, but the choice of the 3mm optical aperture for TLCLs is related to the fact that it is rather difficult to obtain high OP values with larger aperture refractive TLCLs. In the meantime, we have discovered that the combination of a small aperture (3mm) TLCL with a larger aperture (6 mm) fixed lens can provide good quality images (see hereafter). Also, to compensate the distance changes, usually 3D of OP should be enough for the majority of persons, but in some extreme cases,

we can see a need of up to 4D. The requirement on limited scattering (due to possible electrode pixels or molecular orientation thermal fluctuations) is mainly related to the halo effect (to avoid it) during the night driving, etc.

In what follows, we shall try to characterise our lens (as example) and provide answers to key items of the Table 1.

2. Lens design with floating electrode

The schematic (cross section view) of the TLCL, we have developed recently [16], is presented in the Fig. 2(a). The NLC material 1 (Δn≈0.2, thickness ≈50μm) is sandwiched between two substrates (each of 0.1mm thickness). The bottom substrate is covered by a uniform transparent electrode (indium tin oxide, or ITO). The top substrate is covered (from the internal side) by a thin weakly conductive layer (WCL) with ≈10MΩ/sq sheet resistance, which is then covered by a metal layer that is further chemically etched to produce a hole patterned control electrode (HPE, with an internal radius r≈1.5mm). The same top substrate is also covered (from the external side) by an ITO layer that is not controlled (called "floating" electrode, since only the uniform ITO and hole patterned electrodes are actively controlled here). The details of the fabrication of this sandwich may be found elsewhere [16,17].
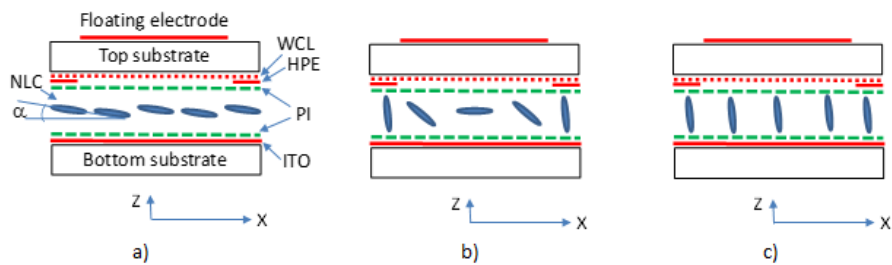
Fig. 2. Schematic (side view) presentation of the TLCL used in the present work. NLC: nematic liquid crystal, WCL: weakly conductive layer, ITO: uniform Indium Tin Oxide, HPE: hole patterned (control) electrode, PI: Polyimide (planar) alignment layers, α: pretilt angle, a) The TLCL is in the ground state (no electric excitation and zero OP), b) The TLCL is excited by a high frequency electric signal (high OP state), c) The TLCL is excited by a low frequency electric signal (zero OP).

The operation principle of the proposed TLCL is as follows: in the absence of the electric field (ground state, Fig. (2a)), all NLC molecules (filled ellipses) are aligned (by means of Polyimide layers [19]) parallel to cell substrates (with a small "pretilt" angle α≈3° [19]) and the refractive index of the sandwich is spatially uniform. Thus, light propagating along the z axis will not be deviated. This state can be called as "passive far field" mode (PFF, with zero OP) for the TLCL (and consequently for the AIOL using it). The application of a high frequency electric signal results into the non-uniform reorientation of molecules (Fig. 2(b)) due to the attenuation of the electric potential when moving from the periphery (HPE, $x = \pm r$) to the center of the lens, $x = 0$ [16,17]. In this case, the effective refractive index of the NLC layer $n_{eff}(x)$ is higher in the center of the TLCL compared to the periphery and thus a gradient is created (along the x axis) that can focus light. The application of a low frequency electric excitation results into a more uniform reorientation of NLC's molecules (since the electric potential propagates from the periphery to the center of the lens with less losses), the refractive index is again uniform (along the x axis, Fig. 2(c)) and light focusing is eliminated. This state can be called as "active far field" (AFF) mode for the AIOL implant.

The addition of the floating electrode [16] is the equivalent of adding a parallel (distributed) capacitive charge in the central part of the lens that accentuates the drop of the electric potential in the center. This helps avoiding the flat central part and decreases the corresponding spherical aberrations. The typical driving technique for such a lens can be found elsewhere [17].

It is important to mention that the NLC being a uniaxial material [12], the cell, described in Fig. 2, will focus only light of extra ordinary polarization (in the plane xz). That is the reason why we call it as "half-lens". We thus need a second similar cell that must be rotated (at 90°) in the plane of substrates (around the z axis) and be attached to the first one (alternative approaches could be considered for very specific application cases [20–24]). In this way, the obtained "double lens" (called "full lens") can focus unpolarised light [18]. If the substrates used are thin enough, two perpendicular polarizations of light will be focused almost on the same plane and there will be no noticeable degradation of the quality of obtained images [17]. All our characterizations (in the current work) are made for full lenses; the photography of a full TLCL with 3mm clear aperture (CA) and an external diameter of 3.5 mm (with two control electrodes; the uniform ITO – grounded and the HPE as a control electrode) is shown at the top inset of Fig. 3.

3. Experimental set-ups and methods

There are various methods to qualify the optical quality of lenses, such as the measurements of the PSF, modulation transfer function (MTF), etc. The bottom part of the Fig. 3 represents schematically the experimental set up that was used in our work to characterize the basic optical properties of our lens by means of a Shack-Hartmann (SH) wavefront sensor (Imagine Optics HASO3-42). The SH wavefront measurement provides Zernike polynomial fits of the wavefront, from which it is very convenient to retrieve different types (more than 7th order) of wavefront aberrations, such as defocus, astigmatism, spherical, coma, etc. The defocus Zernike parameter is directly proportional to the OP of the lens in diopters and allows plotting the OP curve for dynamically tunable lenses vs electrical drive parameters. In the case of the Imagine Optics SH sensor and Zernike coefficients' peak to valley normalization we have

$$OP = Z(3) * 16 / CA^2 \tag{1}$$

where Z(3) is the defocus term in Zernike polynomials and CA is the value of clear aperture's diameter.
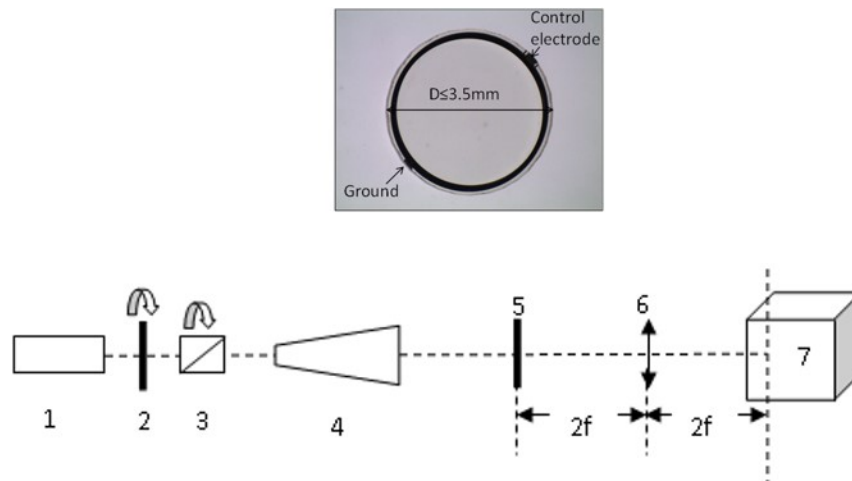
Fig. 3. Schematic presentation of the experimental set-up (bottom) used to measure the OP and aberrations of developed TLCLs (an example of which is shown in the top photo). 1- linearly polarized He-Ne laser; 2- half-wave plate within a rotating holder; 3 – prism of Glan within a rotating holder; 4 - beam expander (X~10); 5- TLCL; 6- imaging lens with 45mm focal length; 7 - Shack-Hartmann wavefront sensor.

Linearly polarized CW He-Ne laser 1 (operating at 632.8nm) was used as probe (Fig. 3). As we have already mentioned, because of the birefringent nature of the NLC, the full TLCL

consisted of 2 LC cells, each one responsible for one linear polarization (for example horizontal and vertical). Therefore, our SH measurements were performed for both polarizations (separately) and averaged thereafter. To control the polarization and the intensity of the incident light, combination of λ/2 plate 2 and Glan prism 3 was used. The transmission axes of the Glan polarizer initially was set parallel to the ground state optical axis' direction of one of the half lenses generating thus an *e* polarized beam inside that cell and then was switched to the perpendicular polarization mode. Beam expander 4 was used to illuminate the entire surface of the TLCL 5. A relay lens 6 (with EFL = 45mm) has imaged (2f + 2f) the output plane of the TLCL 5 onto the SH lenslet array 7.

A second set-up was built to characterize the PSF of our lenses. Figure 4 is the schematic presentation of that setup (bottom) and of a typical photographic image (top photo) of the bright point light source that was used for PSF measurements. To measure the PSF, the extended dynamic range photographic method was used. Namely, the dynamic range of the digital camera (we have used Canon 60D digital camera with 100 mm f/2.8 objective) is not enough to record the entire range of luminance in the PSF. We can overcome this problem by recording a series of images, varying the exposure, and by combining them afterwards to produce an extended dynamic range image that may be analyzed by Matlab and Excel routines to retrieve information on encircled energy (EE) values. We have used Thorlabs' NA = 0.22 & 50μm core diameter multimode fiber 2 as a point light source (pigtailed to a white light source 1). The focus of the digital camera 6 (100mm EFL digital Canon) was manually set to infinity. Tested TLCL 4 was placed just in front of the camera objective using a 3mm hole box/diaphragm 5. In the same time, the diaphragm blocked all environmental light. An achromatic doublet 3 (Thorlabs 200 mm EFL) was used between the fiber tip and the digital camera to compensate the OP of the TLCL by changing the distance between the fiber tip and the achromatic doublet. This distance adjustment was linear with the OP and the fiber tip magnification was constant on the camera sensor.
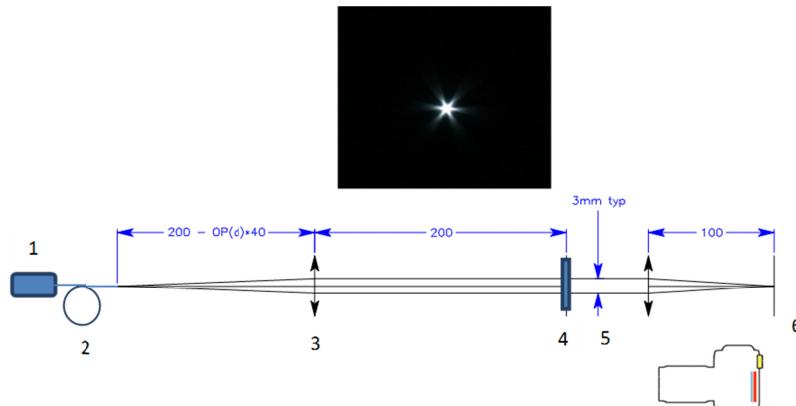
Fig. 4. Schematic presentation of the experimental set-up (bottom) that was used to measure the PSF of the TLCL along with an example (top photo) of the detected intensity distribution. 1: White light source, 2: fiber, 3: achromatic doublet, 4: TLCL under test, 5: diaphragm (∅ = 3mm), 6: digital camera.

A third set-up was built to characterize the transmission and scattering of our lenses (Fig. 5). Those measurements were done by using Ocean Optic (OO) spectrometer USB-4000m UV/VIS, QP600-2-UV/VIS fiber coupled halogen white light source (WLS) HL-2000-Hp, collimating lens, followed by a 3mm diameter diaphragm, integrating sphere (IS) FOIS-1 with ∅ = 10mm diameter opening, sample holder, and a PC with OO software. The light from the WLS and optical fiber was collimated by a lens and directed onto the TLCL under test.

To measure the transmission and the scattering of our TLCL, the distance between the IS's opening and the TLCL was initially set to 90mm, which provides very small acceptance angle ± 3.2° (almost detecting only the specular transmission of light). Then the distance between the IS and TLCL was reduced to approximately 4.5mm, enabling thus the measurement of the total transmission inside of a larger acceptance angle of ± 47.7° (required by ophthalmologists). The scattering value was then calculated as a difference of the above-mentioned transmission values (for ± 47.7° and ± 3.2°). All scattering measurements were done for the entire OP variation range, with 1D steps.
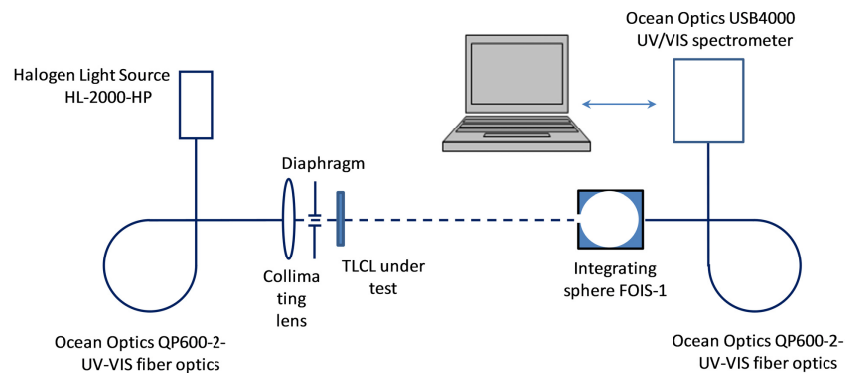
Fig. 5. Schematic presentation of the experimental set-up that was used to measure the transmission and scattering of the TLCL by using an Ocean Optics USB4000 UV/VIS spectrometer.

A fourth set-up was built to characterize the visual perception of images in an imaging system using our TLCL integrated with a Canon camera and a diaphragm of 3mm diameter (simulating an AIOL). The corresponding experimental set-up is shown in Fig. 6. According to the distance from the Canon/TLCL assembly, eye chart targets of different size were printed (on white paper) to provide approximately the same size of images in photographs taken for targets at different distances. Those targets were positioned at different distances and lateral positions enabling their simultaneous photography.
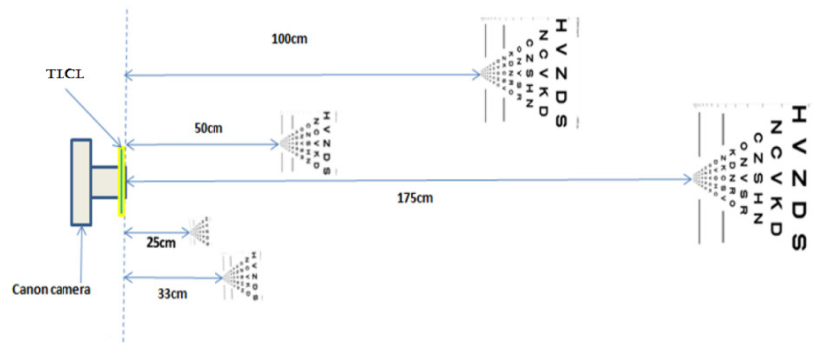
Fig. 6. Schematic presentation of the experimental set-up that was used to record images of targets at different distances with an imaging system using the proposed TLCL (simulating an eye model).

All experiments were performed at room temperature (20°C) unless otherwise identified.

4. Experimental results

We shall further define the difference of the electrically variable portion of the OP from the possible (residual fixed) value of OP in the ground state of the TLCL as "clear" OP (COP). This will be done to exclude the possible contributions of the substrate bending effect on the

OP's analyses. The dynamic range of the obtained OP is presented versus the frequency of driving electrical signal (square shaped AC) in the Fig. 7(a). Those "transfer functions" are obtained for the same TLCL at two different fixed voltage values; U = 3V$_{RMS}$ and U = 4.1V$_{RMS}$. As one can see, the OP of the lens grows continuously with the increase of the frequency and then tends to saturate. The further increase of the frequency results in the slow decrease of the OP and to an increase of its aberrations (Fig. 7(b)). Thus, we shall not analyse that part of frequencies (beyond the maximum of OP). It is important noticing that, while the OP dependences look similar (for two voltage values), the RMS aberrations are very sensitive to the driving voltage (Fig. 7(b)). Thus, the control process can be optimized to obtain minimum possible aberrations (similar optimization was done for the lens-design without the floating electrode [25]). This optimization may involve the choice of "couples" of control parameters: the voltage and the frequency of the driving signal (we shall further call it as V-F control mode).
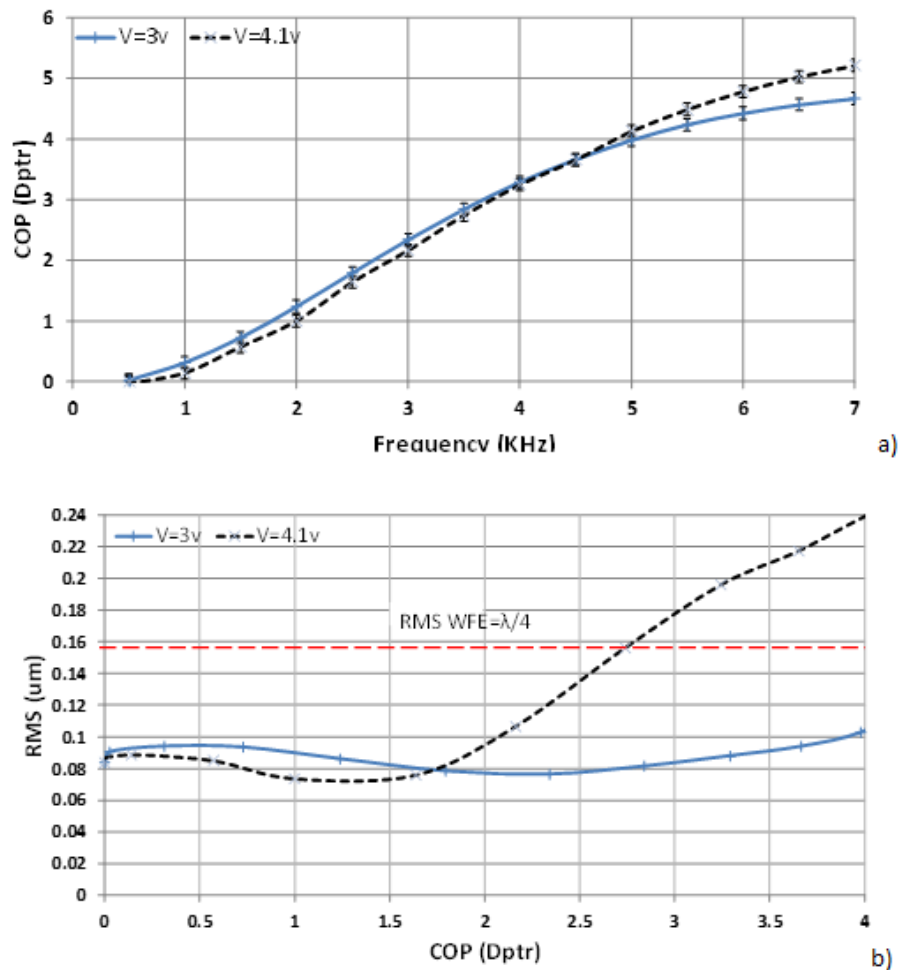
Fig. 7. a) Transfer functions (clear optical power in diopters versus the driving frequency in kHz) of the TLCL for two fixed voltage values (solid line: U = 3V$_{RMS}$ and dashed line: U = 4.1V$_{RMS}$) and b) corresponding RMS aberrations (in μm). The red dashed horizontal line shows the maximum acceptable value for the IOL application.

The intraocular application of such a lens may accept this approach (from the cost point of view) since the temperature of the lens is stable and the added value of distance accommodation may be tremendous. The corresponding trend is presented in the Fig. 8. As

we can see, to obtain the highest possible quality of the lens (with minimal aberrations), the growing OP values will require higher driving frequencies (right vertical axis) and lower voltages (left vertical axis).
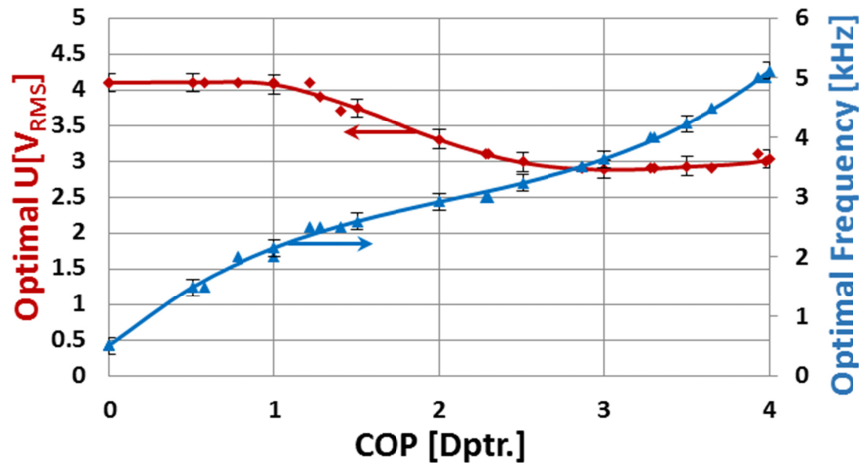
Fig. 8. Optimal driving conditions (voltage and frequency of excitation electric signal) to obtain highest possible optical quality (lowest aberrations) of the TLCL at various COP values in the V-F control mode (see following figures).

As a result, the total root mean square wave front error (RMS WFE) of the lens can be very low. The corresponding results are shown in the Fig. 9. The horizontal dashed line emphasizes the λ/4 level we have mentioned in the Table 1.
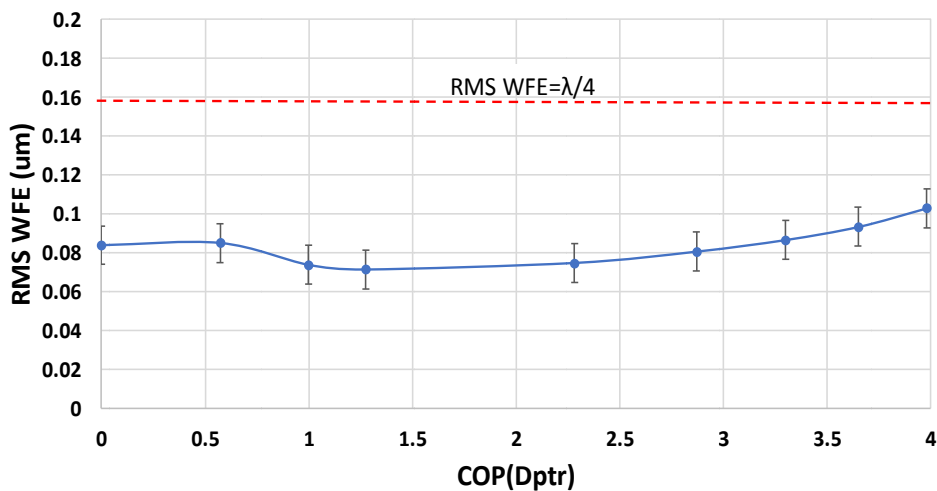
Fig. 9. The total root mean square wavefront error (in μm) for the entire range of COP variation (in Diopters) in the V-F control mode of the TLCL. The red dashed horizontal line shows the maximum acceptable value for the IOL application.

Often, high order RMS WFEs (so called HOA, excluding low order aberrations: astigmatism, coma, trefoil, 3th order spherical aberrations) must be taken into account. We present them separately in the Fig. 10. As we can see, the maximum value of HOA for all

COP values is <0.067μm. Here also, the horizontal dashed line emphasizes the 0.1μm level we have set in the Table 1.

We have also analyzed the PSF of our TLCL. We have started by measuring the portion of the energy enclosed within various solid angles corresponding to the PSF spot for each OP values. An example of such measurement is shown in the Fig. 11(a) for active far field (the energy was integrated within a solid angle the cross section value of which is presented on the horizontal axes). We have then extracted the Fractional Energy versus the PSF spot's diameter (Fig. 11(b)). As we can see, the TLCL's performance satisfies the 20/20 vision target according to which the 85% of EE's angular "radius" should not exceed 2arcminutes (corresponding to 1.16mrad). The obtained PSF 85% EE angular radius is 1.72arcmin, which is 3.6% more than the value obtained for the active far field (1.66arcmin). It is worth mentioning that the maximum allowed difference is ≈5%. The dashed horizontal line shows the maximum acceptable value of the angular radius of 85% EE. As we can see, the performance of the lens is good up to approximately 3.5D (almost over the entire dynamic range).
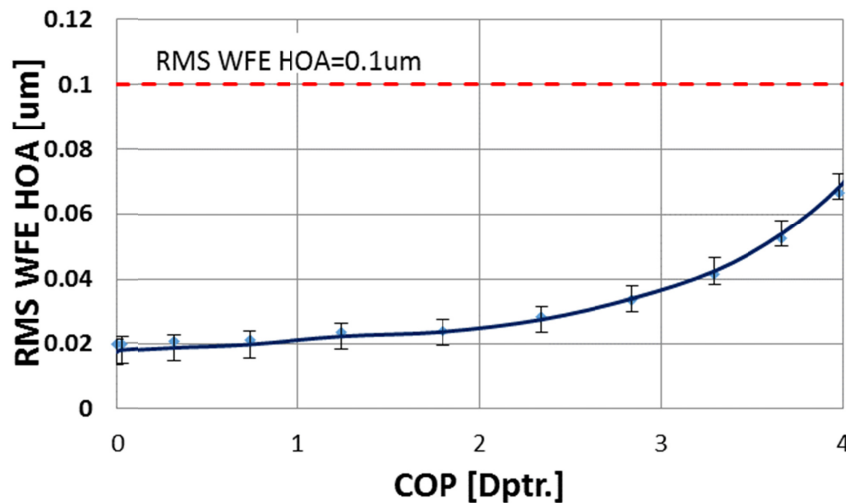
Fig. 10. High order root mean square aberrations (RMS WFE HOA in μm) versus the COP (in Diopters) for the V-F control mode. The red dashed horizontal line shows the maximum acceptable value for the IOL application.

The measurement of optical transmission is another key requirement for LC based imaging or vision components. The reason for that is the absorption of LC materials in the short wavelength region as well as the relatively high scattering (due to orientational molecular fluctuations [12]), which is also more pronounced for short wavelengths. In the particular case of the proposed TLCL, losses are also defined by the absorption of the WCL and of the ITO as well as by Fresnel reflections from multiple interfaces (air-glass, glass-ITO, etc.). The transmission tests here were performed for TLCLs that had several index matching layers (for internal interfaces) as well as broad band anti reflection coatings for both external (air-glass and glass-air) interfaces. The corresponding results are shown in the Fig. 12 for the AFF state of the lens (Fig. 2(c)), that is, for a 4.1V, 0.5 kHz drive signal, which corresponds to 0D of OP. The spectrally averaged (between 450 nm and 650 nm) specular transmission is above 90% (the opening of the integrating sphere is ∅ = 10mm and it was placed at 90mm distance from the sample).
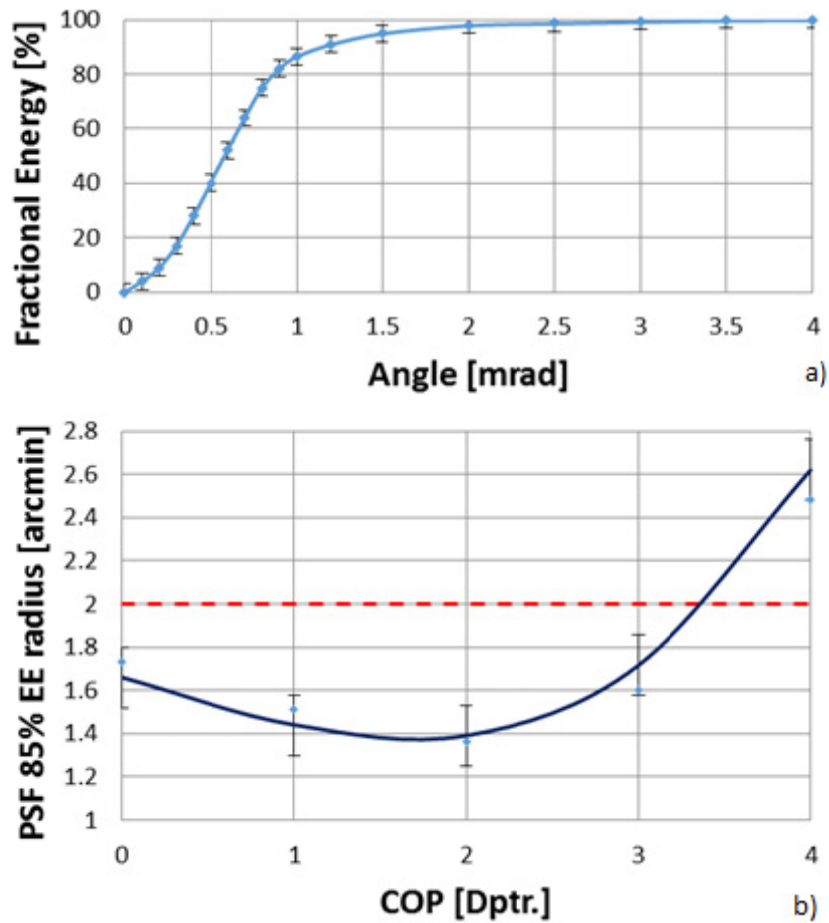
Fig. 11. a) Fractional Energy versus the angle corresponding to the PSF spot's diameter. b) The radius of 85% encircled energy (EE) vs the COP of the TLCL. The red dashed horizontal line shows the maximum acceptable value for the IOL application.
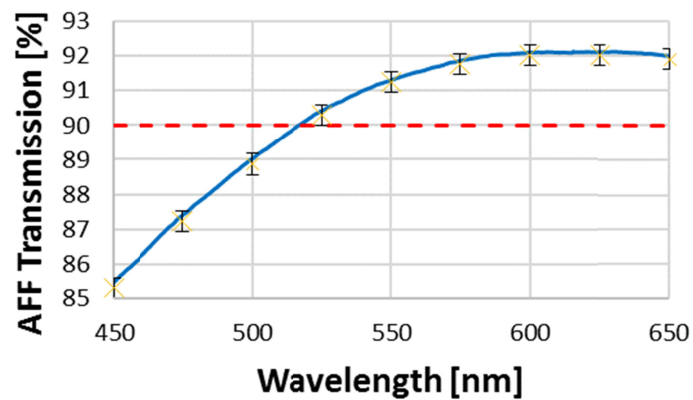
Fig. 12. Spectral dependence of specular transmission of the TLCL in the active far field state (0.5 kHz, 4.1V). The red dashed horizontal line shows the minimum acceptable value for the IOL applications.

The measurement of scattering is particularly important for ophthalmic (intraocular or other) implants since many of them (particularly multifocal IOLs) are suffering from starburst and halo during the night driving. This necessarily suppose that the object is further than the dashboard. Thus, the most important state corresponds to the zero OP. However, we have also measured the large scattering for other OP values too; the same setup was used since the distance changes (from 4.5mm to 90mm) we have performed were much shorter than the shortest focal distance of our lens F = 250mm. The obtained results, describing the scattering level of our lens, are shown in the Fig. 13. As we can see, for all OP levels, the scattering values remain below maximum acceptable value of 5.5%.
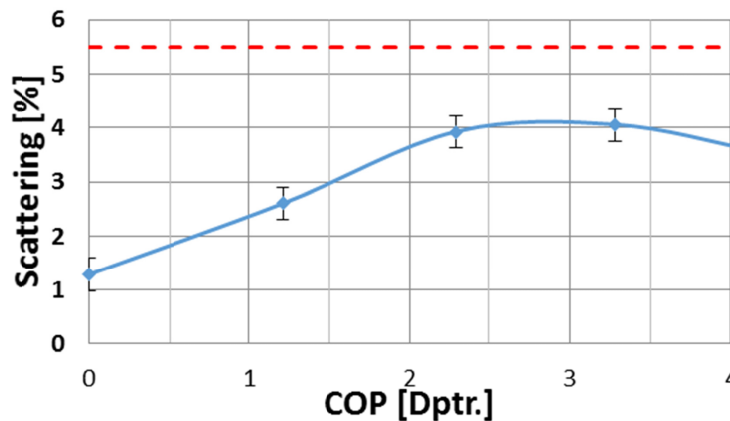
Fig. 13. Spectrally averaged (from 450 nm to 650 nm) light scattering value for the entire variation range of the COP of the TLCL. The red dashed horizontal line shows the maximum acceptable value for the IOL application.

Table 2 shows in more details the values of spectrally averaged scattering in various operation modes.

Table 2. Spectrally averaged light scattering by TLCL at various regimes.

Scattering (± 0.2%)	Voltage (V_{RMS})	Frequency (kHz)	Info
2.3%	0	N/A	Passive Far Field (max 3.6% allowed)
1.4%	4.1	0.5	Active Far Field (max 2.5% allowed)
3.6%	3	5.1	Averaged scatttering at 4D
4.1%	2.9	3.5	Maximum averaged scattering

Concerning the visual perception experiments (see Fig. 6), to simulate the operation of a fixed monofocal IOL (see the line 1, Fig. 14), we have recorded photographic images by using the following procedure: the OP of the imaging system was set for one specific value (e.g., at zero OP of the TLCL used for far distance observation, column entitled 0D). Obviously, the image in the far position (first line) appears to be clear in this case. All other images of the first line, positioned at different (closer) distances, appear blurry, since their observation (with high quality) would require additional OP, described in each column (1D for 1m distance, 2D for 0.5m, 3D for 0.33m and 4D for the 0.25m).

To simulate the operation of a multifocal IOL (see the second line, Fig. 14), we have performed only one additional adjustment of the OP (by adding a fixed focus lens of appropriate OP) enabling the observation at two positions (here, at far field, requiring 0D of

OP and at 0.33 m, requiring 3D of OP, for example, for screen observation task). As a result, all other images (targets positioned at 1m, 0.5m and 0.25 m) appear blurry.

Finally, to simulate the operation of an AIOL with our TLCL, we have simply adjusted the control parameters of the TLCL to optimize the contrast at all observation distances and the corresponding results are presented in the last line of the Fig. 14. As we can see, the quality of images is good at all distances and this process is continuous (not limited only to those 4 discrete distances). It is worth mentioning that, if the person would have many examples of fixed focus glasses (here, at least 4 units with various OPs), then we should compare all 5 images of the last raw with the left image of the first raw. Obviously transporting many glasses is not a very practical option.
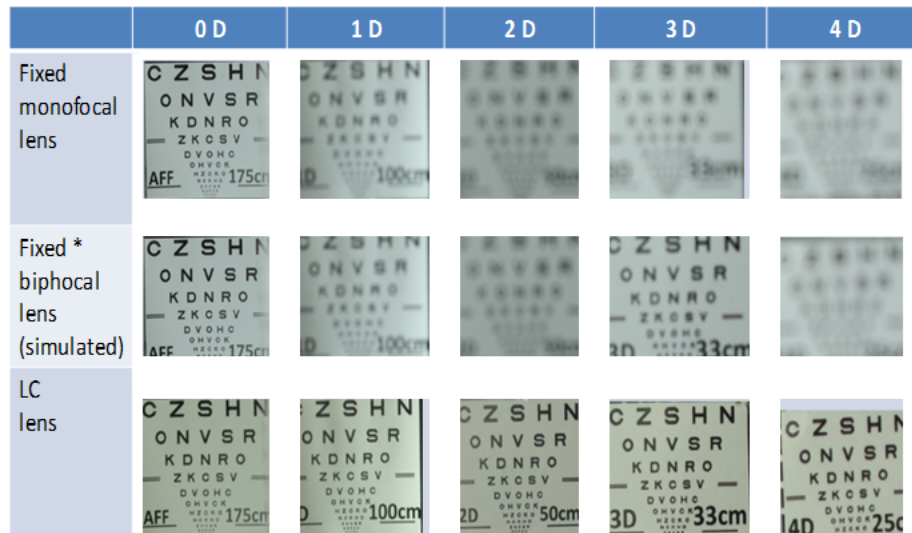
Fig. 14. Images recorded by using the imaging system with integrated TLCL (using the experimental set up presented in Fig. 6).

5. Discussions and conclusions

Given that the developed TLCL is an electrically variable gradient index (or GRIN) lens, its OP's variability range decreases quadratically with the increase of its radius r (see Eq. (1) and [17,26–28]). While the quality of images obtained with a system combining the TLCL of 3mm CA with the Canon camera is very good at all distances (Fig. 13), if desired, we could fabricate such TLCLs with larger CA also. For example, we could increase the CA above 4mm with still an OP $\approx$2.3D that is enough to cover the majority of accommodation needs. Further increase of CA (with still acceptable OP values) is possible in the framework of a single aperture refractive lens design (as the one presented here) if the application can tolerate some more aberrations and more scattering. Other approaches of CA's increase (that applies a double zone (Fresnel type) refractive lens or an additional ring-shaped electrode, or a lens with curved gap, etc.) have been demonstrated also ([13,29–31]). Such an increase might be interesting for contact lens [31] or augmented reality applications [32,33]. The introduction of additional electrodes or the segmentation of electrodes ([13,19,34]) may be used to enhance the capability of our lens to change the aberrations of the lens and of the AIOL. Thus, it may be possible to remotely correct/adjust the age-related natural changes of eye aberrations for the patient bearing the implant [7].

Another important aspect is the electrical power consumption of the lens when we are targeting portable implants (such as AIOL or accommodative contact lenses). Our lens assembly can be described as a capacitive charge the power consumption P of which can be expressed as

$$P \approx 2FCV^2 \tag{2}$$

where F if the driving frequency, C is the capacitance (the experimentally measured value is $C \approx 100\text{pF}$) and V is the voltage. When the lens is activated ($V \geq 0$), we can consider two extreme cases of operation; far and close distances. Referring on the Fig. 7(a), the value of P can thus be estimated to be $P \approx 1\mu\text{W}$ for the AFF (at 0.5 kHz, corresponding to OP = 0) and $P \leq 10\mu\text{W}$ for the close distance (5kHz for 4D, 3V). The experimentally measured value for the close distance operation (high OP) was indeed $P \approx 10\mu\text{W}$. Thus, as it can be estimated (from the Eq. (2)), the power consumption of this TLCL ranges from 1μW (active far focus) to 10μW (close focus). Obviously, the passive far field does not consume power. We think that this is an excellent performance.

The use of a WCL imposes some temperature dependence of control parameters. The detailed analyses of our lens at 35°C has shown (not reported here for the sake of shortness) that all performance parameters remain similar with only one change; the frequency of the driving signal must be increased by approximately 60%. This will slightly increase also the power consumption of the lens. In addition, we have to take into account also the power consumption of the driving circuit, which obviously depends upon the type of the circuit and is out of the scope of the present work.

Additional experiments performed (not reported here) have shown that the entire cycle of distance accommodation (close-far-close) is indeed below 1 sec. It is worth noticing that the use of the frequency as a control parameter allows the development of new driving regimes where the frequency jumps can be used (in addition to voltage kicks) to perform fast transitions between different values of OP ([35,36]).

We did not perform separate studies of the halo generated by our lens since such investigations have been conducted in parallel [37] and the obtained results have shown that the performance of our lens is quite comparable with the monofocal IOLs (noticeably better compared to the performance of multifocal IOLs).

It is worth noticing that the proposed TLCL has also excellent performance in terms of space utilisation. Indeed, as we can see from the Fig. 3, the clear aperture diameter is representing ≈86% of the external diameter of the lens (compared to other electrically variable solutions where this ratio may drop down to 30%).

It is also interesting to notice that many lens designs might be difficult to transfer into production. In contrast, the proposed design of the lens is easily manufacturable even in old "second generation" LC display manufacturing lines. The panel fabrication of such lenses (thousands of such lenses on the same panel) was successfully performed (1.5% of lens-to-lens standard deviation in the OP variability range).

Finally, the "elephant in the room" is the question "how the focusing distance may be identified and communicated to the TLCL?". To address this problem, we have developed and theoretically validated a very promising technique where the variations of inductive coupling of coils (in each eye implant) can be used for this purpose [38].

In conclusion, we think that the presented results (analyses of the TLCL with floating electrode) have shown that the optical performance of this lens design is excellent in almost all aspects that are important for the ophthalmic application (see Table 1).

References

1. K. Richdale, M. A. Bullimore, and K. Zadnik, "Lens thickness with age and accommodation by optical coherence tomography," Ophthalmic Physiol. Opt. **28**(5), 441–447 (2008).
2. J. L. Alió, J. L. Alió Del Barrio, and A. Vega-Estrada, "Accommodative intraocular lenses: where are we and where we are going," Eye Vis. (Lond.) **4**(1), 16–27 (2017).
3. R. B. Melles, J. T. Holladay, and W. J. Chang, "Accuracy of intraocular lens calculation formulas," Ophthalmology **125**(2), 169–178 (2018).
4. H. S. Ong, J. R. Evans, and B. D. Allan, "Accommodative intraocular lens versus standard monofocal intraocular lens implantation in cataract surgery," Cochrane Database Syst. Rev. **5**, CD009667 (2014).
5. J. V. Forrester, A. D. Dick, P. G. McMenamin, F. Roberts, and E. Pearlman, *The Eye E-Book: Basic Sciences in Practice* (Elsevier Health Sciences, 2015).
6. G. Vdovin, M. Loktev, and A. Naumov, "On the possibility of intraocular adaptive optics," Opt. Express **11**(7), 810–817 (2003).
7. T. Galstian and H. Earhart, "Reprogrammable tuneable liquid crystal lens intraocular implant and methods therefor," US patent 20160106533 (2016).
8. G. Li, P. Valley, P. Ayras, D. Mathine, S. Honkanen, and N. Peyghambarian, "High-efficiency switchable flat diffractive ophthalmic lens with three-layer electrode pattern and two-layer via structures," Appl. Phys. Lett. **90**(11), 111105 (2007).
9. P. Clark, T. Galstian, K. Asatryan, , V. Presniakov, A. Bagramyan, A. Tork, A. Zohrabyan, and S. Careau, "Methods and apparatus for focus improvement in multiple liquid crystal cell lenses," US patent US14777086 (2016).
10. T. Galstian, "Tuneable liquid crystal lens intraocular implant and methods therefor," US Patent 13/369,806 (2018).
11. L. M. Blinov and V. G. Chigrinov, *Electrooptic effects in liquid crystal materials* (Springer Science & Business Media, 2012).
12. P.-G. de Gennes and J. Prost, *The physics of liquid crystals* (Oxford University Press, 1995).
13. O. Sova and T. Galstian, "Liquid crystal lens with optimized wavefront across the entire clear aperture," Opt. Commun. **433**, 290–296 (2019).
14. H. E. Milton, P. B. Morgan, J. H. Clamp, and H. F. Gleeson, "Electronic liquid crystal contact lenses for the correction of presbyopia," Opt. Express **22**(7), 8035–8040 (2014).
15. A. F. Naumov, M. Yu. Loktev, I. R. Guralnik, and G. Vdovin, "Liquid-crystal adaptive lenses with modal control," Opt. Lett. **23**(13), 992–994 (1998).
16. T. Galstian, K. Asatryan, V. Presniakov, A. Zohrabyan, A. Tork, A. Bagramyan, S. Careau, M. Thiboutot, and M. Cotovanu, "High optical quality electrically variable liquid crystal lens using an additional floating electrode," Opt. Lett. **41**(14), 3265–3268 (2016).
17. T. Galstian, O. Sova, K. Asatryan, V. Presniakov, A. Zohrabyan, and M. Evensen, "Optical camera with liquid crystal autofocus lens," Opt. Express **25**(24), 29945–29964 (2017).
18. T. V. Galstian, *Smart mini-cameras* (CRC Press, 2013).
19. L. Begel and T. Galstian, "Liquid crystal lens with corrected wavefront asymmetry," Appl. Opt. **57**(18), 5072–5078 (2018).
20. T. Galstian and K. Allahverdyan, "Focusing unpolarized light with a single-nematic liquid crystal layer," Opt. Eng. **54**(2), 025104 (2015).
21. C.-T. Lee, Y. Li, H.-Y. Lin, and S. T. Wu, "Design of polarization-insensitive multi-electrode GRIN lens with a blue-phase liquid crystal," Opt. Express **19**(18), 17402–17407 (2011).
22. Y. Li and S.-T. Wu, "Polarization independent adaptive microlens with a blue-phase liquid crystal," Opt. Express **19**(9), 8045–8050 (2011).
23. S.-H. Lin, L.-S. Huang, C.-H. Lin, and C.-T. Kuo, "Polarization-independent and fast tunable microlens array based on blue phase liquid crystals," Opt. Express **22**(1), 925–930 (2014).
24. R. Bao, C. Cui, S. Yu, H. Mai, X. Gong, and M. Ye, "Polarizer-free imaging of liquid crystal lens," Opt. Express **22**(16), 19824–19830 (2014).
25. A. Naumov, G. Love, M. Y. Loktev, and F. Vladimirov, "Control optimization of spherical modal liquid crystal lenses," Opt. Express **4**(9), 344–352 (1999).
26. J. W. Goodman, *Introduction to Fourier optics* (Roberts and Company Publishers, 2005).
27. Y.-H. Lin, Y.-J. Wang, and V. Reshetnyak, "Liquid crystal lenses with tunable focal length," Liq. Cryst. Rev. **5**(2), 111–143 (2017).
28. G. Li, "Adaptive lens," Prog. Opt. **55**, 199–283 (2010).
29. T. Galstian, K. Asatryan, V. Presniakov, A. Bagramyan, A. Zohrabyan, and S. Careau, "Flat liquid crystal layered fresnel lens device," patent WO2017197533A1 (2018).
30. A. Jamali, D. Bryant, Y. Zhang, A. Grunnet-Jepsen, A. Bhowmik, and P. J. Bos, "Design of a large aperture tunable refractive Fresnel liquid crystal lens," Appl. Opt. **57**(7), B10–B19 (2018).
31. H. E. Milton, P. B. Morgan, J. H. Clamp, and H. F. Gleeson, "Electronic liquid crystal contact lenses for the correction of presbyopia," Opt. Express **22**(7), 8035–8040 (2014).
32. H.-S. Chen, Y.-J. Wang, P.-J. Chen, and Y.-H. Lin, "Electrically adjustable location of a projected image in augmented reality via a liquid-crystal lens," Opt. Express **23**(22), 28154–28162 (2015).

33. Y.-H. Lee, G. Tan, T. Zhan, Y. Weng, G. Liu, F. Gou, F. Peng, N. V. Tabiryan, S. Gauza, and S.-T. Wu, "Recent progress in Pancharatnam–Berry phase optical elements and the applications for virtual/augmented realities," Opt. Data Process. Storage **3**(1), 79–88 (2017).
34. L. Begel and T. Galstian, "Dynamic compensation of gradient index rod lens aberrations by using liquid crystals," Appl. Opt. **57**(26), 7618–7621 (2018).
35. T. Galstian, O. Sova, K. Asatryan, V. Presniakov, A. Zohrabyan, and M. Evensen, "Optical camera with liquid crystal autofocus lens," Opt. Express **25**(24), 29945–29964 (2017).
36. T. Galstian, P. P. Clark, T. C. Antognini, J. J. Parker, D. A. Paroudian, T. Killick, and A. Zobhrabyan, Autofocus system and method, US patent US12542458 (2014).
37. K. Sperlich, T. Koch, S. Bohn, H. Stolz, R. F. Guthoff, T. Galstian, and O. Stachs, "Study on glare phenomena and vision quality of a virtually implanted tunable liquid crystal IOL compared to monofocal and EDOF IOLs," in *The Association for Research in Vision and Ophthalmology Annual Meeting* (ARVO, 2019).
38. T. Galstian and D. Brousseau, Inductive coil sensor for vision corrective apparatus and methods therefro, US patent US14956145 (2016).